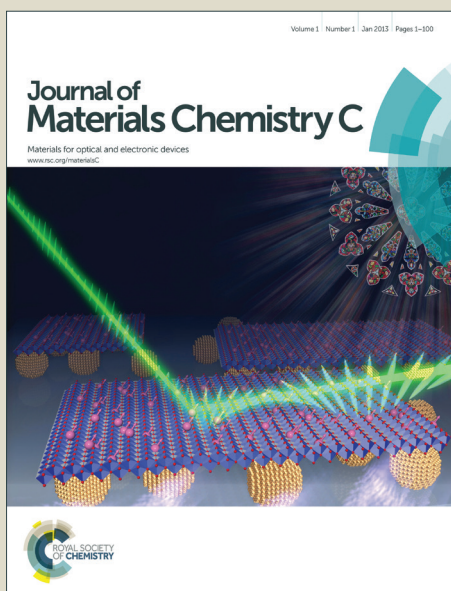


Journal of Materials Chemistry C

Accepted Manuscript



This is an *Accepted Manuscript*, which has been through the Royal Society of Chemistry peer review process and has been accepted for publication.

Accepted Manuscripts are published online shortly after acceptance, before technical editing, formatting and proof reading. Using this free service, authors can make their results available to the community, in citable form, before we publish the edited article. We will replace this *Accepted Manuscript* with the edited and formatted *Advance Article* as soon as it is available.

You can find more information about *Accepted Manuscripts* in the [Information for Authors](#).

Please note that technical editing may introduce minor changes to the text and/or graphics, which may alter content. The journal's standard [Terms & Conditions](#) and the [Ethical guidelines](#) still apply. In no event shall the Royal Society of Chemistry be held responsible for any errors or omissions in this *Accepted Manuscript* or any consequences arising from the use of any information it contains.

Dual light-emitting nanoparticles: second harmonic generation combined with rare-earth photoluminescence

Ludovic Mayer,^{†‡} Géraldine Dantelle,^{†} Vincent Jacques,^{‡*} Sandrine Perruchas,[†] Gilles Patriarche,[§] Jean-François Roch^{*} and Thierry Gacoin[†]*

[†] Laboratoire de Physique de la Matière Condensée, Ecole Polytechnique - CNRS, UMR 7643, 91128 Palaiseau Cedex, France.

[‡] Laboratoire de Photonique Quantique et Moléculaire – ENS Cachan - CNRS, UMR 8537, 94235 Cachan, France.

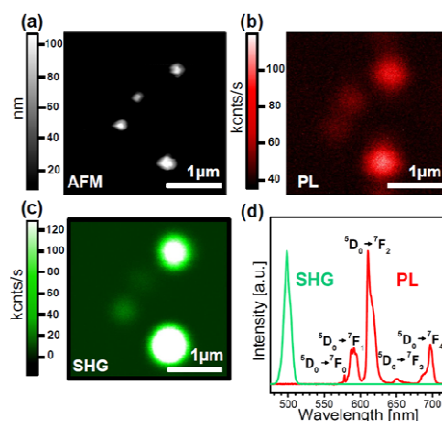
^{*} Laboratoire Aimé Cotton, CNRS UPR 331, Université Paris-Sud and ENS Cachan, 91405 Orsay Cedex, France.

[§] Laboratoire de Photonique et Nanostructures, CNRS UPR 20, Route de Nozay, 91460 Marcoussis, France.

KEYWORDS. Core shell nanoparticle, second harmonic generation, photoluminescence, lanthanide doping.

ABSTRACT Dual emitting KTP@LaPO₄:Eu nanoparticles have been synthesized and characterized. These core@shell heterostructures, consisting of a KTP (KTiOPO₄) single-crystal core and a Eu³⁺-doped LaPO₄ shell were synthesized by a coprecipitation method and controlled heterogeneous nucleation of LaPO₄:Eu around the KTP nanocrystals. These nanoparticles exhibit both the SHG (second harmonic generation) signal of the KTP core and the PL (photoluminescence) emission of the doping europium ions of the shell. The orientation-dependent signal of SHG in contrast with the PL emission has been demonstrating through a detailed optical study at the single particle level. This property makes these dual emitting systems original nanoproboscopes for studying dynamic systems in biology. The versatility of the developed method can be straightforwardly adapted to other lanthanide ions to develop new multifunctional nanoproboscopes.

TOC GRAPHICS



Introduction.

The development of light-emitting nanoparticles with multi-functional properties is a key issue for optical microscopy applied to biology and life science. Pioneering works were achieved on quantum dots, showing their large potentialities for localization and tracking experiments at the single particle level¹. Besides down-converting fluorescent nanoparticles and systems emitting through non-linear phenomena such as up-conversion^{2,3}, compounds emitting via two photon excitation or second harmonic generation (SHG) are the subject of an increasing number of studies⁴. These emitters can be coherently excited by a two-photon process with infrared wavelength, thus preventing tissues degradation and leading to improved spatial resolution due to the quadratic excitation process. Concerning the specific case of SHG nanoemitters, additional properties rely on the possible non-resonant excitation enabling saturation-free photostable emission and the possible orientation tracking⁵. Increasing numbers of systems have been studied in the last few years, mainly based on materials known in the bulk state for their interesting SHG properties. BaTiO₃^{6,7,8}, KNbO₃⁹, Fe(IO₃)₃¹⁰ and KTiOPO₄ (KTP)¹¹ nanoparticles have been elaborated, exhibiting almost the same properties of the bulk materials. In particular, Hsieh *et al.* demonstrate the possibility to image 90-nm non-centrosymmetric BaTiO₃ nanoparticles deposited onto a glass substrate, using efficient second-harmonic generation signal¹². Similarly, Bonacina *et al.* report the high SHG emission of 80-nm Fe(IO₃)₃ nanocrystals spread onto a substrate. Such studies pave the way to the use of these systems as bio-markers. As a proof of concept, we recently succeeded in internalizing and imaging KTP nanocrystals into cortical neurons¹³.

A particularly appealing property of the SHG nanoparticles is the possibility of orientation tracking based on the polarization-dependent SHG signal. Indeed, the components of the second-order susceptibility vary according to the orientation of the nanocrystal with the respect to the

incident electric field^{5,11}. In biology, this feature is interesting in order to follow dynamic phenomena such as molecular motors in microtubules for instance¹⁴. However, as the intensity of the detected SHG signal depends on the nanoparticle orientation, the optical signal can disappear as the particle moves, a phenomenon which is then detrimental for *in situ* biological tracking. This effect can be compensated by using a reference signal which remains constant whatever the particle orientation. For this purpose, one strategy is to combine in the same nanoparticle the SHG signal with a classical non polarization-dependent luminescence emission signal. To our knowledge, in the literature, no other study reports the preparation of nanoparticles emitting both by SHG and photoluminescence.

Here, we present our investigation concerning the development of dual emitting nanoparticles exhibiting both SHG and photoluminescence (PL) light emission properties. By taking advantage of our previous works on SHG KTP nanoparticles¹³ and on luminescent rare-earth doped oxide particles,¹⁵ nanoparticles of KTP associated with europium ions as luminescent emitters have been synthesized. In a first approach, we studied the case of direct doping of KTP particles by Eu^{3+} ions. Based on the very low doping content obtained, we then considered the case of core@shell nanoparticles in which the core consisting of a KTP crystal is encapsulated with a $\text{LaPO}_4:\text{Eu}$ luminescent shell. The synthesis, structural and optical characterizations of these nanoparticles, namely $\text{KTP}@\text{LaPO}_4:\text{Eu}$, are presented. A study at the single nanoparticle level confirms their combined SHG properties and characteristic lanthanide emission. These nanoprobables exhibiting dual emission properties open new potentialities for the development of biological labels with orientation tracking functionality.

Results and discussion.

In a recent study, we have developed the synthesis of single-crystal KTP nanoparticles which are highly stable in aqueous media and exhibit the outstanding SHG properties of the bulk materials¹³. This synthesis is based on a coprecipitation method followed by a thermal treatment allowing the formation of perfectly crystalline nanoparticles. Our first approach to obtain dual emitting nanoparticles was the direct incorporation of europium ions within the KTP lattice.

Bulk flux-grown KTP single-crystals were doped with lanthanide ions (Nd^{3+} , Tb^{3+} , Ho^{3+} , Er^{3+} , Tm^{3+} , and Yb^{3+}) with the goal of modifying their physical properties (improvement of the ionic conductivity, reduction of the KTP cutoff wavelength) and of finding new applications for solid-state laser technology^{16,17}. Although the lanthanide doping concentration remained low (138 ppm for Nd^{3+} doping¹⁸), the incorporation of lanthanide ions in the KTP matrix appeared to be effective. To our knowledge, there is no report in the literature of such doping at the nanoscale. Note that BaTiO_3 nanoparticles were doped with lanthanide ions but the SHG properties of these systems were not reported^{19,20}.

Thus, we simply adapted our KTP synthesis¹³ by replacing part of the titanium precursor ($\text{Ti}(\text{OBU})_4$) with europium salt (EuCl_3) in the 0.1 to 10 mol% range (experimental part). Structural characterizations (powder X-Ray diffraction, HAADF-STEM, EDX in Figures S1) of the product showed no difference between undoped KTP nanoparticles for low doping concentrations, whereas for higher Eu contents ($> 1\%$) a parasitic phase is formed. The composition of this phase seems to arise from a mixture of KPO_3 and EuPO_4 . These results show no or very low incorporation of Eu^{3+} ions within the KTP nanoparticles but instead their segregation in a separate phase. These results can be explained by the difference in the ionic radius and the charge state of the Eu^{3+} ions and those of the K^+ and Ti^{4+} in the host KTP

structure. At the difference of a flux synthesis which brings enough energy to force the incorporation, our low-temperature synthesis method does not lead to an effective incorporation of Eu^{3+} into the KTP matrix.

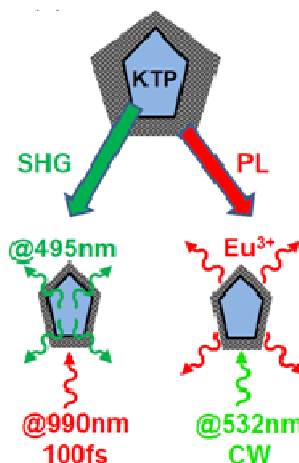


Figure 1. Schematic representation of the core@shell nanoparticles with a KTP nanocrystal covered with Eu^{3+} ions in a LaPO_4 matrix and the expected optical response.

Another strategy was then adopted consisting in the synthesis of core@shell nanoparticles. In these heterostructures, the SHG-emitting KTP core is covered with a shell of luminescent material as illustrated in Figure 1. The advantage of this nanostructure is that the KTP structure is kept intact without perturbation of the crystallinity which is a crucial parameter for preserving the SHG properties⁵. Indeed, J.J. Carvajal *et al.* who succeeded in doping RTiOPO_4 single-crystals with up to 1 mol% Yb^{3+} by adding Nb^{5+} co-dopant for charge compensation sake, observed a decrease of the SHG efficiency due to internal strains²¹. LaPO_4 was chosen as the shell compound because this oxide can be easily doped with trivalent lanthanide ions leading to highly luminescent materials^{22,23,24}. Its other advantages are its well-controlled synthesis in solution and the fact that its phosphate nature can ensure a good affinity with the KTP core

particles whose high negative zeta potential ($\xi = -45$ mV in water) has been attributed to surface PO_4^- groups. The doping concentration was chosen at 5 mol% Eu^{3+} to avoid any concentration quenching. $\text{LaPO}_4:\text{Eu}$ can be excited in the UV range, *i.e.* in a transition corresponding to the charge-transfer Eu-O band or in the visible range, *i.e.* in the f-f Eu transitions (typically at 395 nm corresponding to the ${}^7\text{F}_0-{}^5\text{D}_3$ transition). The Eu^{3+} ions can also be optically excited using a commercially available 532-nm laser, with the resonance towards the ${}^5\text{D}_1$ excited states²³. This green excitation will minimize the absorption from tissues, an important feature for biology experiments.

In order to favor heterogeneous nucleation of the $\text{LaPO}_4:\text{Eu}$ phase over homogeneous one, the shell deposition has been carried out under slow kinetic conditions. The synthesis has been conducted in aqueous solution by reacting $\text{La}(\text{NO}_3)_3$ and $\text{Eu}(\text{NO}_3)_3$ (5 mol%) salts with tripolyphosphate ($\text{Na}_5\text{P}_3\text{O}_{10}$) in the presence of KTP nanoparticles with a mean diameter of 150 nm serving as seeds (experimental details in SI). The thermal hydrolysis of tripolyphosphate slowly releases the phosphate ions²⁴, leading to the progressive precipitation of $\text{LaPO}_4:\text{Eu}$ compound around the KTP nanoparticles. Thus, by an accurate control of the precursor concentration and the reaction temperature, the formation of a $\text{LaPO}_4:\text{Eu}$ shell around the KTP nanoparticles was successfully obtained as observed by TEM (Figure 2). In order to get a significant shell amount, the deposition process was repeated twice. As shown in Figure 2c, the 150-nm KTP nanoparticles are thus coated with a ~ 10 nm thick shell. No homogeneous nucleation of the shell compound is observed. In Figure 2d, the shell appears rough and polycrystalline with small crystalline grains (< 10 nm) while the KTP single crystal in the core remains unaffected. This is in accordance with the PXRD analysis (Figure S2) showing only the diffraction peaks corresponding to the KTP structure. The small coherence length of shell

compound does not allow its detection. The presence of a shell is confirmed by DLS (Dynamic Light Scattering) measurements showing an increase of the particle mean diameter of 25 nm (Figure S3), in agreement with the synthesis of a shell of about 10 nm thickness (Figure 2). This analysis also demonstrates the stability of the core@shell nanoparticles in aqueous solution as no aggregation is detected. The zeta-potential value of $\xi = -40$ mV confirms the good colloidal stability and is due to the phosphate groups at the particle surface in accordance with pure $\text{LaPO}_4:\text{Eu}$ nanoparticles ($\xi = -30$ mV)²⁵.

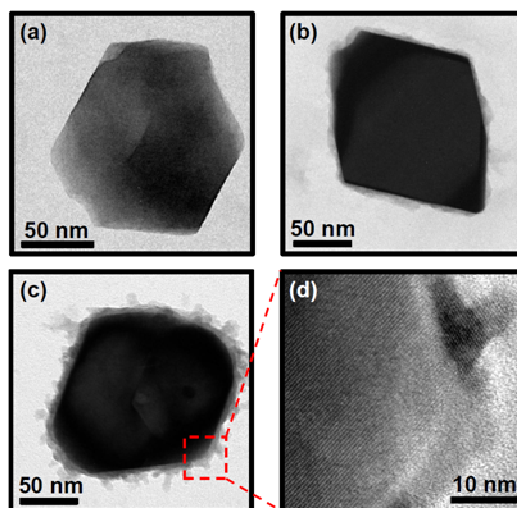


Figure 2. TEM images of core@shell nanoparticles at different steps of the synthesis. (a) Image of a typical KTP nanoparticle used as seeds. (b) Image of a $\text{KTP@LaPO}_4:\text{Eu}$ 5 % nanoparticle after a first shell deposition and (c) after a second shell deposition. (d) HRTEM image of the shell corresponding to the red dashed square area on (c).

STEM analysis was performed on these $\text{KTP@LaPO}_4:\text{Eu}$ nanoparticles to accurately analyze their structure and composition (Figure 3). The roughness of the oxide shell is obviously observed in Figure 3a in the HAADF mode. Concerning the composition, the K and Ti chemical

maps overlap (Figures 3b-c), while the areas of P, La and Eu are larger (Figure 3d-e-f), proving the formation of a core/shell system. Quantitative EDX spectroscopy performed on the different particles exhibits a K/Ti ratio of 1, in good agreement with the formation of the KTiOPO_4 phase. Considering a Ti/P ratio of 1, a P/La ratio of ~ 1.5 is found, which can be explained by the formation of the LaPO_4 phase and the presence of additional phosphate surface groups, according to the synthesis conditions (synthesis in presence of tripolyphosphate in excess to favor the colloidal stability). The Eu/La ratio is found to be ~ 0.02 , which is in the range of the 0.05 value of the concentrations used.

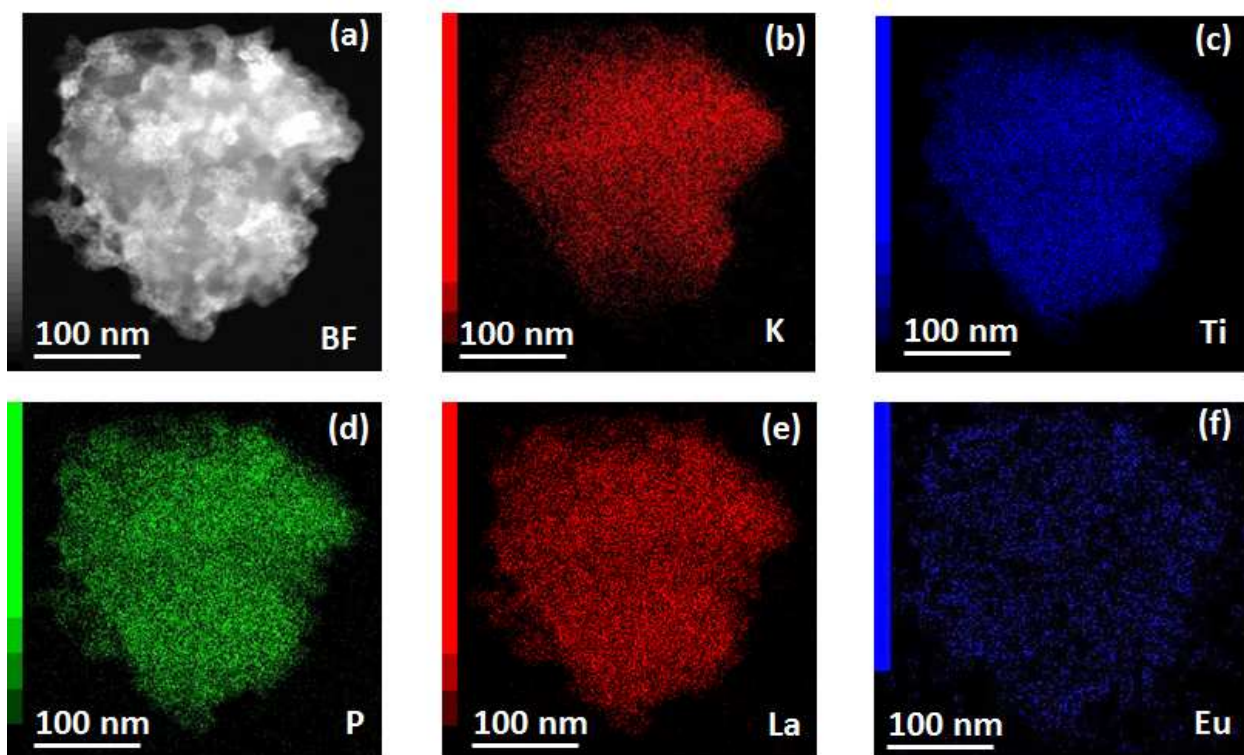


Figure 3. STEM-EDX images of $\text{KTP@LaPO}_4:\text{Eu}$ nanoparticles. (a) HAADF imaging. (b) EDX K chemical map. (c) Ti chemical map. (d) P chemical map. (e) La chemical map. (f) Eu chemical map.

The photoluminescence (PL) properties of the colloidal suspension of KTP@LaPO₄:Eu nanoparticles have then been studied at the macroscopic level. The emission spectrum recorded with an excitation wavelength of 395 nm presents the classical characteristics of Eu³⁺ luminescence with the ⁵D₀ to ⁷F_J (J = 0-6) emission lines (Figure 4). The area ratio between the ⁵D₀ - ⁷F₂ electric dipole emission band and the ⁵D₀ - ⁷F₁ magnetic dipole emission band is known to be characteristic of the symmetry of the environment²⁶. For perfectly crystalline rhabdophane LaPO₄:Eu, an area ratio near unity for those two lines is observed²², while a ratio of ~2.5 is observed in our case. The discrepancy indicates that the LaPO₄ shell has a low crystallinity, either intrinsic or due to the high specific surface as suggested from the TEM images.

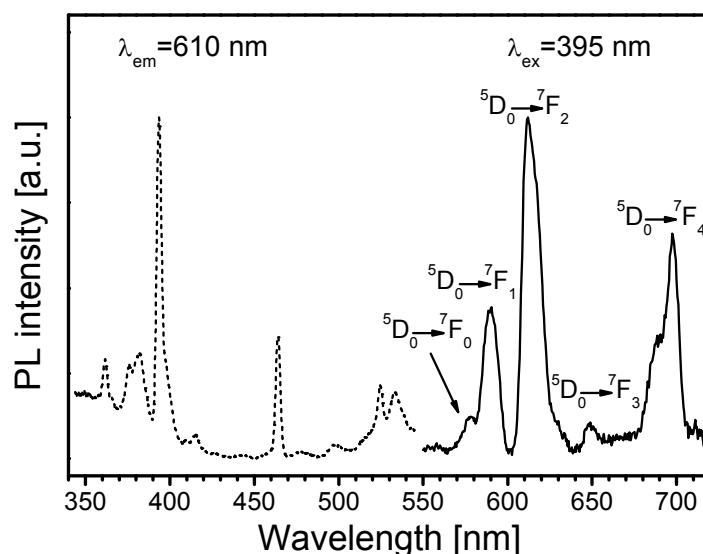


Figure 4. Optical properties of a colloidal solution of KTP@LaPO₄:Eu nanoparticles: in solid line, photoluminescence spectrum under an excitation at 395 nm and in dashed line, excitation spectrum for an emission at 610 nm.

In order to investigate the optical properties of KTP@LaPO₄:Eu nanoparticles at a single particle level, a customized two-photon optical microscope coupled with an atomic force

microscope (AFM) was used (Figure S4). Laser excitation lines can be switched to either observe the SHG from the KTP core (femtosecond laser $\lambda_{\text{ex}} = 990$ nm, 100 fs pulse duration, 86 MHz repetition rate, 1 mW mean power) or the photoluminescence (PL) from the shell (CW laser $\lambda_{\text{ex}} = 532$ nm, 10 mW). This experimental set-up allows us to correlate the SHG and PL signal intensities with the size of each spotted nanoparticle as shown in Figure 5. For this experiment, the $\text{KTP@LaPO}_4\text{:Eu}$ nanoparticles were deposited on a quartz substrate and about 20 particles were individually analyzed. As an example, the AFM, PL and SHG images of 4 nanoparticles are shown in Figures 5a-c and corresponding data are reported in Table 1.

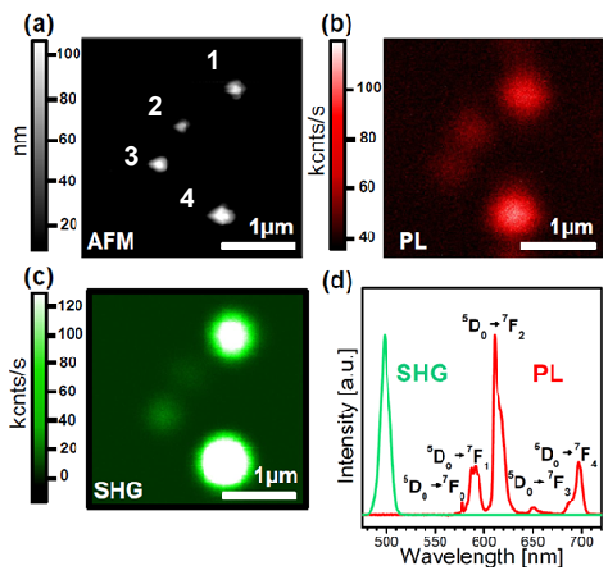


Figure 5. Optical study of the core-shell $\text{KTP@LaPO}_4\text{:Eu}$ nanoparticles at the single particle level. (a) AFM imaging, (b) PL imaging, (c) SHG imaging and (d) mean emission spectra for PL (red curve) and SHG (green curve) for 25 nanoparticles. PL peaks are labeled corresponding to the $^5\text{D}_0$ to $^7\text{F}_j$ emission lines of Eu^{3+} .

Particle	Average particle radius (nm)	SHG intensity (kcounts/s)	PL intensity (kcounts/s)
n°1	120	309.6	34.6
n°2	47	3.9	19.2
n°3	111	25.8	12.3
n°4	147	886.4	46.8

Table 1. AFM, SHG and PL data for the KTP@LaPO₄:Eu nanoparticles of Figure 5. The average particle radius has been estimated by AFM by taking the average dimensions in the z- and x- directions.

For each nanoparticle observed in the AFM map, both SHG and PL were successfully detected with neither bleaching nor blinking. The evolution of both SHG and PL intensities as a function of the pump power is reported on Figure S5. It reveals the linear variation of the PL intensity as well as the quadratic evolution of the SHG signal. Moreover, no quenching effect is evidenced in this system.

The PL spectrum of individual nanoparticles was recorded (Figure 5d and Figure S6). Taking into account the difference of spectrometer resolution, these spectra are similar to the one recorded for the colloidal solution (Figure S6). This result suggests that the shell chemical composition is homogeneous from one particle to another.

The SHG signal from a single-crystal nanoparticle with sub-wavelength size is the coherent response of all atoms in the KTP core, which builds an induced dipole oscillating at the frequency 2ω . Its components are associated to the second-order susceptibility tensor coefficients of the bulk KTP crystal and to the incident electric field oscillating at the frequency ω according to:

$$P_i^{2\omega} = \varepsilon_0 \sum_{j,k} \chi_{ijk}^{(2)}(-2\omega, \omega, \omega) E_j^\omega E_k^\omega$$

where i , j , and k , span the Cartesian coordinates in the laboratory frame, respectively along the (x,y) transverse axis and the z longitudinal optical axis^{11,13}. By rotating the input linear polarization of the excitation laser, a dipolar-type response associated to the radiated second-harmonic intensity is then observed and can be used to retrieve the crystalline orientation of the nanocrystal⁵. The SHG polar response measured along the x and y transverse axis for one $\text{KTP@LaPO}_4\text{:Eu}$ nanoparticle is shown in Figure 6. A dipolar signal is observed confirming the single-crystal character of the KTP core. To retrieve the orientation of the corresponding nanoparticle, the data were fitted and the following Euler angles obtained are $\theta = 94^\circ$, $\varphi = 94^\circ$ and $\psi = 59^\circ$, as defined in Figure 6a. A similar analysis has been performed on each other nanoparticle.

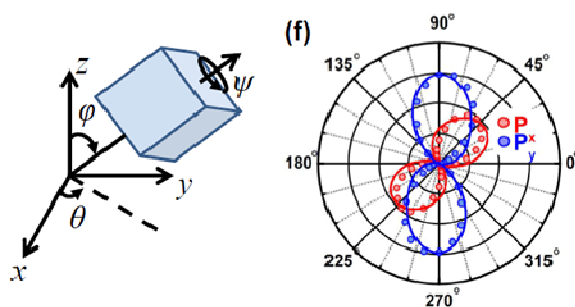


Figure 6. (a) Euler angles definition associated to the nanocrystal orientation. (b) Experimental SHG polar response measured along x (red dots) and y (blue dots) transverse axis emission for one $\text{KTP@LaPO}_4\text{:Eu}$ nanoparticle. Data are fitted (solid lines) to retrieve the crystalline orientation of the KTP core.

Strong variations of SHG intensity between particles can be noted (Table 1). Taking into account a simple model of spherical particles with an average radius R_{av} , estimated by the mean value of x and z values determined by AFM, the particle volume V was calculated. As SHG signal depends on V^2 , the variation of the SHG intensity was plotted as a function of V^2 for a set

of nanoparticles (Figure S7). No trend can be determined, as explained by the fact that SHG is also polarization-dependent and the randomness of the nanoparticle orientations on the substrate explains the uncorrelated data.

Considering a homogeneous LaPO₄ coating, the evolution of the PL intensity was plotted as a function of R_{av}^2 for 16 particles including the four shown on Figure 5 (Figure S8). In contrast with SHG, the PL signal is directly correlated with the quantity of LaPO₄:Eu, as expected from an incoherent radiation of independent emitters.

Considering this model and a background noise of 3 kcts/s, the detection limit for photoluminescence corresponds to a spherical particle with a diameter of ~80 nm, in the conditions described here. Although the emission intensity varies linearly with the excitation power up to saturation, it is not possible to work at higher excitation power as the strong fluorescent background arising from the quartz substrate would be detrimental for the PL detection. For the SHG signal, it was previously reported that particles as small as 25 nm could be easily detected when the particle is well-oriented¹³.

Hence the KTP@LaPO₄:Eu system combines the advantages of SHG signal and those of PL emission: SHG detection allows a detection of smaller particles than PL, however it is strongly dependent on the particle orientation on the contrary to PL.

Conclusion

We report here the successful development of KTP@LaPO₄:Eu dual emitting nanoparticles. These core@shell structures exhibit both the SHG signal of the KTP core and the PL emission of the doping europium ions of the shell. This method has the advantage of not altering the crystalline KTP core, thus allowing a highly sensitive SHG detection at the single particle level.

Thanks to the well-controlled synthesis of LaPO₄ in solution, good colloidal stability has been obtained. A single particle level optical study demonstrates the orientation-dependent signal of SHG in contrast with the PL one. This study opens the way to the use of these dual emitting nanoprobes for biological applications for studying dynamic systems. Moreover, the versatility of the method developed here can be straightforwardly adapted to other lanthanide ions. For instance, doping with Yb³⁺ and Er³⁺ can be envisioned to combine up-conversion luminescence with SHG using only one excitation wavelength, or with Gd³⁺ to develop a multifunctional nanoprobe for applications combining optical microscopy and MRI.

ASSOCIATED CONTENT.

Supporting Information

“This material is available free of charge via the Internet at <http://pubs.acs.org>.”

AUTHOR INFORMATION

Corresponding Author

*Email: geraldine.dantelle@polytechnique.edu

ACKNOWLEDGMENT

We acknowledge fruitful discussions with Michel Simmoneau (INSERM 894, Paris).

REFERENCES

¹ Pinaud, F., Clarke, S., Sittner, A., Dahan, M. *Nature Methods* **2010**, *7*, 275-285

-
- ² Mialon, G., Turckan, S., Dantelle, G., Collins, D. P., Hadjipanayi, M., Taylor, R. A., Alexandrou, A., Gacoin, T. & Boilot, J.-P. *J. Phys. Chem. C* **2010**, *114*, 22449-22454
- ³ Yi, G.S., Chox, G. M. *Chem. Mater.* **2007**, *19*, 341
- ⁴ Zipfel, W.R., Williams, R.M., Webb, W.W. *Nature Biotechnology* **2003**, *21*, 1369
- ⁵ Brasselet, S.; Le Floch, V.; Treussart, F.; Roch, J.-F.; Zyss, J.; Botzung-Appert, E. and Ibanez, A. *Phys. Rev. Lett.* **2004**, *92*, 207401
- ⁶ Hellwarth, R. and Christensen, R. *Appl. Opt.* **1975**, *14*, 247-248
- ⁷ Hsieh, C.-L., Grange, R., Pu, Y. and Psaltis, D. *Biomaterials* **2010**, *31*, 2272-2277.
- ⁸ Pantazis, P., Maloney, J., Wu, D. & Fraser, S. E. *Proc. Natl. Acad. Sci. USA* **2010**, *107*, 14535-14540.
- ⁹ Nakayama, Y., Pauzauskie, P. J., Radenovic, A., Onorato, R. M., Saykally, R. J., Liphardt, J. & Yang, P. *Nature* **2007**, *447*, 1098-1101
- ¹⁰ Bonacina, L., Mugnier, Y., F. Courvoisier, F., Le Dantec, R., Extermann, J., Lambert, Y., Galez, C. & Wolf J.-P. *Appl. Phys. B* **2007**, *87*, 399-403
- ¹¹ Le Xuan, L., Zhou, C., Slablab, A., Chauvat, D., Tard, C., Perruchas, S., Gacoin, T., Villeval, P. & Roch, J.-F. *Small* **2008**, *4*, 1332-1336
- ¹² Hsieh, C.L., Grange, R. Pu, Y., Psaltis, D. *Opt. Express* **2009**, *17*, 2880
- ¹³ Mayer, L., Slablab, A., Dantelle, G., Jacques, V., Bestel, A.M., Perruchas, S., Spinicelli, P., Thomas, A., Chauvat, D., Simmoneau, M., Gacoin, T., Roch, J.F. *Nanoscale* **2013**, *5*, 8466
- ¹⁴ Sanchez, T., Chen, D. T. N., DeCamp, S. J., Heymann, M., Dogic, Z. *Nature* **2012**, *491*, 431-434
- ¹⁵ Bouzigues, C., Gacoin, T. and Alexandrou, A. *ACS Nano* **2011**, *5*, 8488-8505
- ¹⁶ Solé, R., Nikolov, V., Koseva, I., Peshev, P., Ruiz, X., Zaldo, C., Martin, M. J., Aguilo, M., Diaz, F. *Chem. Mater.* **1997**, *9*, 2745
- ¹⁷ Zaldo, C., Rico, M., Diaz, F., Carvajal, J.J. *Opt. Mater.* **1999**, *13*, 175
- ¹⁸ Zaldo, C., Rico, M., Martin, M.J., Masson, J., Aguilo, M., Diaz F. *J. Lumin.* **1998**, *79*, 127
- ¹⁹ Culver, S.P., Stepanov, V., Mecklenburg, M., Takahashi, S., Brutchey, R.L. *Chem. Comm.* **2014**, *50*, 3480
- ²⁰ Rabuffetti, F.A., Culver, S.P., Lee, J.S., Brutchey, R.L. *Nanoscale* **2014**, *6*, 2909

-
- ²¹ Carvajal, J.J., Solé, R., Gavalda, J., Massons, J., Aguilo, M., Diaz, F. *Opt. Mater.* **2003**, *24*, 425
- ²² Meysamy, H., Riwotzki, K., Kornowski, A., Naused, S., Haase, M. *Ad. Mater.* **1999**, *11*, 840
- ²³ Riwotzki, K., Meysamy, H., Kornowski, A., Haase, M. *J. Phys. Chem. B* **2000**, *104*, 2824
- ²⁴ Buissette, V., Moreau, M., Gacoin, T., Boilot, J.P., Chane-Ching, J.Y., Lemerrier, T. *Chem. Mater.* **2004**, *16*, 3767
- ²⁵ Buissette, V., Moreau, M., Gacoin, T., Boilot, J.P. *Adv. Funct. Mater.* **2006**, *16*, 351
- ²⁶ Zollfrank, C., Scheel, H., Brungs, S., Greil, P. *Crystal Growth and Design* **2008**, *8*, 766